

Supporting Information

Hysteresis Effect on Carrier Transport and Photoresponse

Characteristics in Hybrid Perovskites

Tiqiang Pang^{a, c}, Kai Sun^{a, b}, Yucheng Wang^d, Suzhen Luan^e, Yuming Zhang^a, Yuejin Zhu^b, Ziyang Hu^{*, b} and Renxu Jia^{*, a}

^a School of Microelectronics, Xidian University, Key Laboratory of Wide Band-Gap

Semiconductor Materials and Devices, Xi'an 710071, China.

^b Department of Microelectronic Science and Engineering, Ningbo University, Ningbo, 315211, China

^c Department of Physics, Chemistry and Biology (IFM) Linköping University, Linköping, 58183, Sweden

^d School of Microelectronics, Northwestern Polytechnical University, Xi'an 710072, China

^e Xi'an University of Science and Technology, Xi'an 710054, China

Corresponding Authors

* E-mail address: rxjia@mail.xidian.edu.cn.

* E-mail address: huziyang@nbu.edu.cn.

METHOD

One-dimensional diffusion equation was solved numerically using the Crank-Nicholson algorithm.

$$\frac{\partial n(x,t)}{\partial t} = D \frac{\partial^2 n(x,t)}{\partial x^2} - k(t) \cdot n(x,t) \quad (\text{S1})$$

For convenience, the $n(x, t)$ appearing in the following text is all replaced by n , and the constant $k(t)$ is replaced by k . Discretize the Equation (S1), which can be obtained:

$$\frac{n_i^{j+1} - n_i^j}{\Delta t} = \frac{D}{2(\Delta x)^2} [n_{i+1}^{j+1} - 2n_i^{j+1} + n_{i-1}^{j+1}] + [n_{i+1}^j - 2n_i^j + n_{i-1}^j] - \frac{k}{2} (n_i^{j+1} + n_i^j) \quad (\text{S2})$$

Move Δt on the left side of the Equation (S2) to the right side of the equation, then:

$$n_i^{j+1} - n_i^j = \frac{D \cdot \Delta t}{2(\Delta x)^2} [n_{i+1}^{j+1} - 2n_i^{j+1} + n_{i-1}^{j+1}] + [n_{i+1}^j - 2n_i^j + n_{i-1}^j] - \frac{k \cdot \Delta t}{2} (n_i^{j+1} + n_i^j) \quad (\text{S3})$$

Note: $\alpha = \frac{D \cdot \Delta t}{2(\Delta x)^2}$, $\beta = \frac{k \cdot \Delta t}{2}$, Substituting α and β into Equation (S3), then:

$$n_i^{j+1} - n_i^j = \alpha [n_{i+1}^{j+1} - 2n_i^{j+1} + n_{i-1}^{j+1}] + [n_{i+1}^j - 2n_i^j + n_{i-1}^j] - \beta (n_i^{j+1} + n_i^j) \quad (\text{S4})$$

Move the item containing n^{j+1} in Equation (S4) to the left side of the equation, and the item containing n^j to the right side of the equation, it can be seen,

$$-\alpha \cdot n_{i-1}^{j+1} + (1 + 2\alpha + \beta) n_i^{j+1} - \alpha \cdot n_{i+1}^{j+1} = \alpha \cdot n_{i-1}^j + (1 - 2\alpha - \beta) n_i^j + \alpha \cdot n_{i+1}^j \quad (\text{S5})$$

Matrix Equation (S5), then:

$$[A \begin{bmatrix} n^{j+1} \end{bmatrix}] = [B \begin{bmatrix} n^j \end{bmatrix}] + [C] \quad (\text{S6})$$

$$[n^{j+1}] = \begin{bmatrix} n_{11}^{j+1} \\ n_{12}^{j+1} \\ n_{13}^{j+1} \\ n_{21}^{j+1} \\ n_{22}^{j+1} \\ n_{23}^{j+1} \\ n_{31}^{j+1} \\ n_{32}^{j+1} \\ n_{33}^{j+1} \end{bmatrix} \quad [n^j] = \begin{bmatrix} n_{11}^j \\ n_{12}^j \\ n_{13}^j \\ n_{21}^j \\ n_{22}^j \\ n_{23}^j \\ n_{31}^j \\ n_{32}^j \\ n_{33}^j \end{bmatrix}$$

$$[A] = \begin{bmatrix} A1 & 0 & 0 \\ 0 & A1 & 0 \\ 0 & 0 & A1 \end{bmatrix} \quad [B] = \begin{bmatrix} B1 & 0 & 0 \\ 0 & B1 & 0 \\ 0 & 0 & B1 \end{bmatrix}$$

$$[A1] = \begin{bmatrix} 1+2\alpha+\beta & -\alpha & 0 \\ -\alpha & 1+2\alpha+\beta & -\alpha \\ 0 & -\alpha & 1+2\alpha+\beta \end{bmatrix}$$

$$[B1] = \begin{bmatrix} 1-2\alpha-\beta & \alpha & 0 \\ \alpha & 1-2\alpha-\beta & \alpha \\ 0 & \alpha & 1-2\alpha-\beta \end{bmatrix}$$

$$[C] = \begin{bmatrix} \alpha(n_{11}^{j+1} + n_{11}^j) \\ 0 \\ 0 \\ \alpha(n_{22}^{j+1} + n_{22}^j) \\ 0 \\ 0 \\ \alpha(n_{33}^{j+1} + n_{33}^j) \\ 0 \\ 0 \end{bmatrix}$$

$$[n^{j+1}] = [A^{-1}][B][n^j] + [C]$$

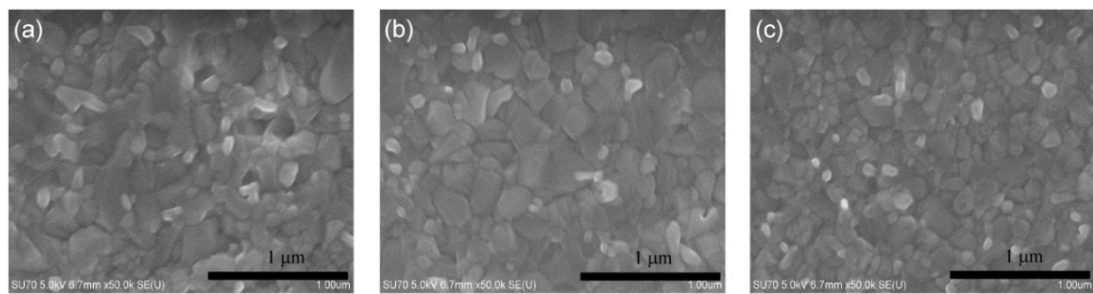


Figure S1. Top-view SEM images of undoped and doped perovskites. (a) pure PVK, (b) PVK(I), (c) PVK(PCBM). The size bar is 1 μm .

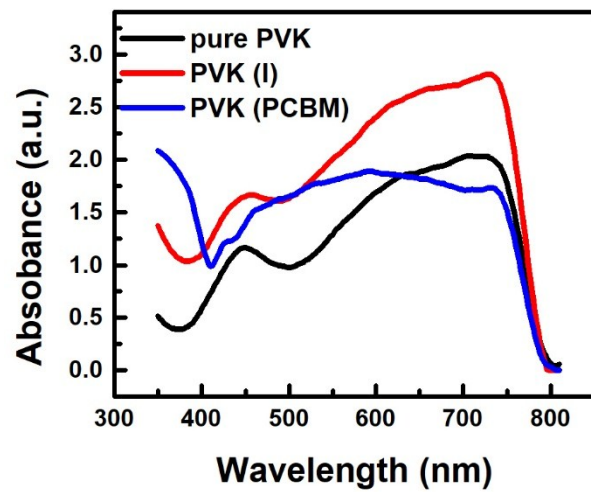


Figure S2. UV-visible absorption spectra of the perovskites. Note: absorption of substrate was not removed.

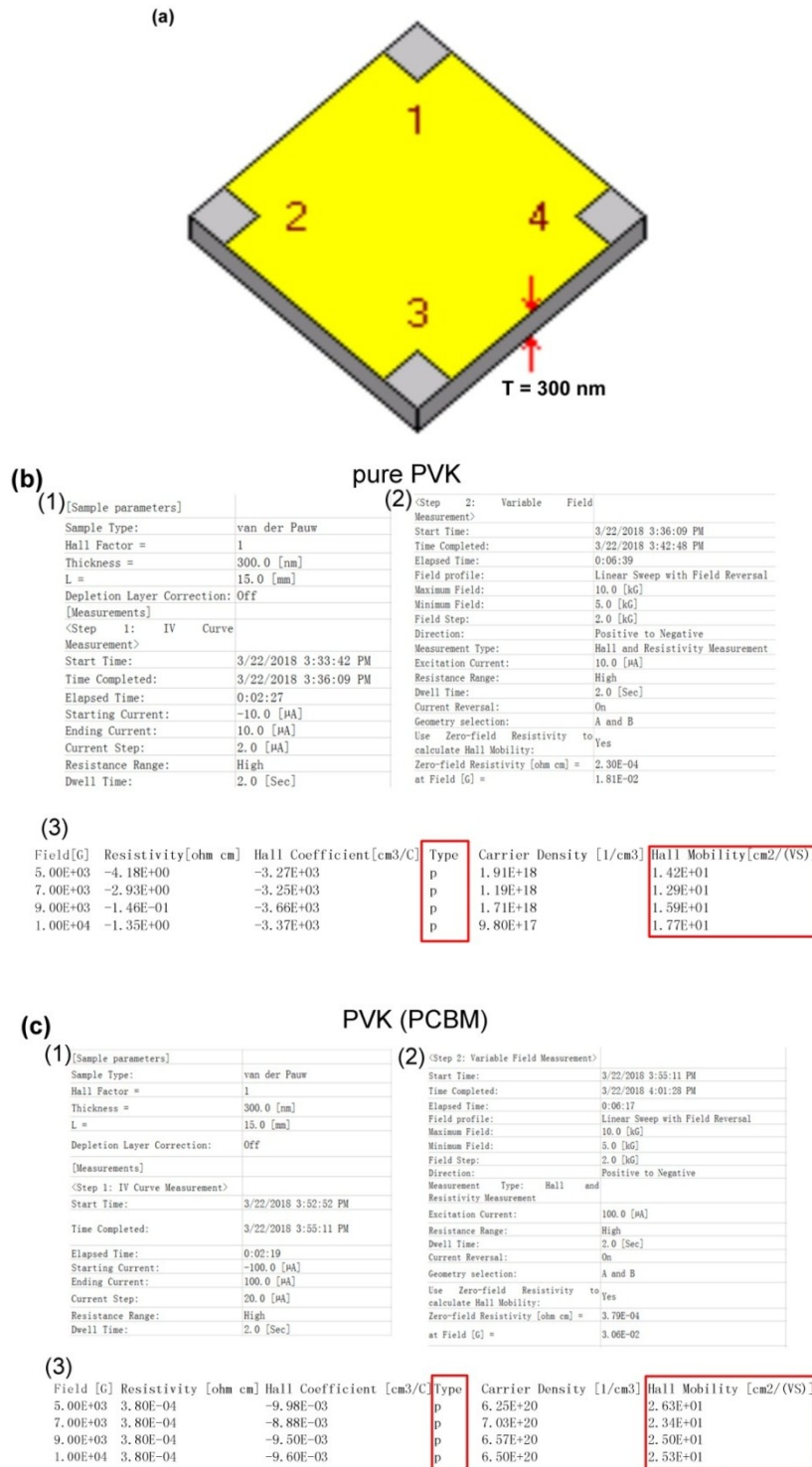


Figure S3. Hall effect measurement results. (a) Sample structure. The thickness of the perovskite film is 300 nm, the sample size is 1.5 cm × 1.5 cm, and four metal electrodes are grown by physical vapor deposition around the sample, and the electrode size is 0.3 cm × 0.3 cm. (b) pure PVK (c) PVK(PCBM). (1), (2) and (3) represents sample parameters, variable field measurement and result information, respectively.

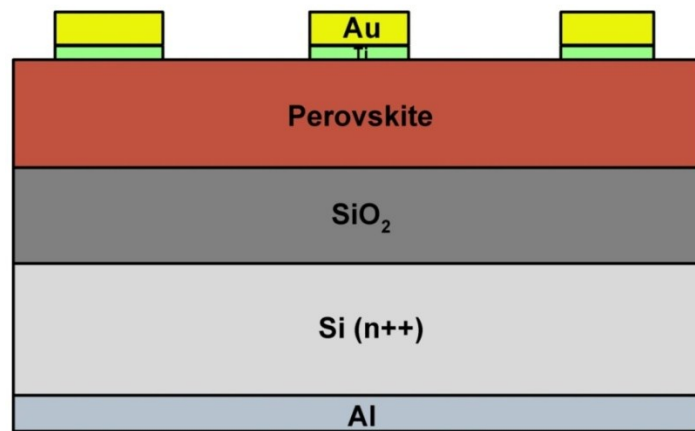


Figure S4. Structure schematic of the perovskite based MOS capacitor.

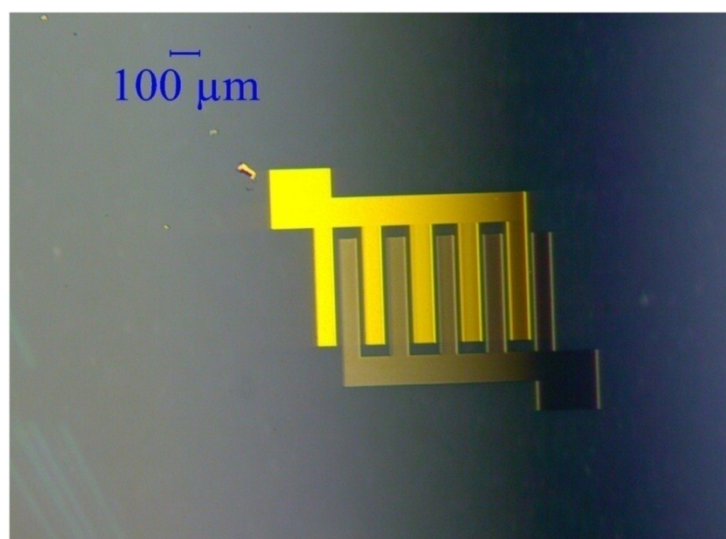


Figure S5. Lithography pattern of interdigitated electrodes based MSM structure.

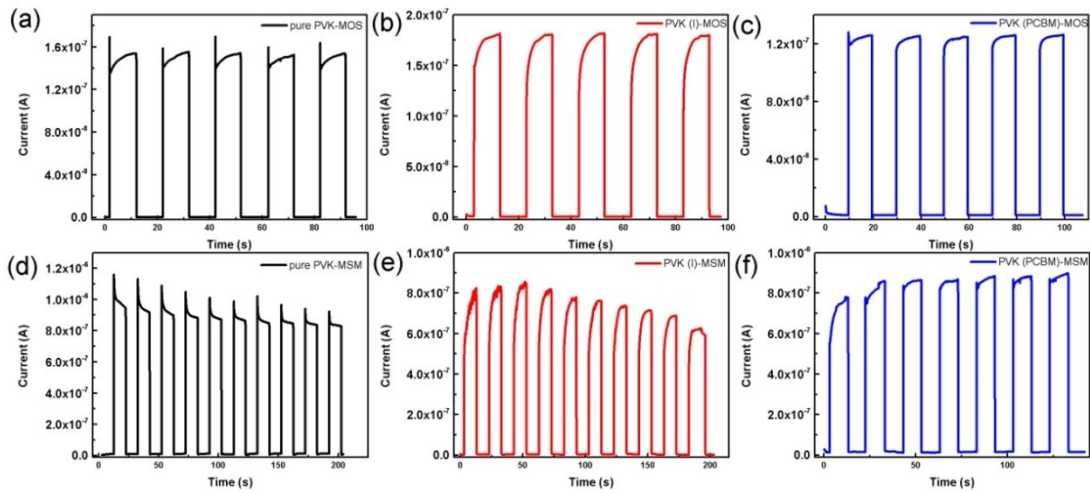


Figure S6. I-t characteristic curves of photodetectors illuminated with a light intensity of $5 \text{ mW}\cdot\text{cm}^{-2}$ obtained by ON/OFF switching at 5 V. (a) pure PVK based MOS structure photodetectors. (b) PVK(I) based MOS structure photodetectors. (c) PVK(PCBM) based MOS structure photodetectors. (d) pure PVK based MSM structure photodetectors. (e) PVK(I) based MSM structure photodetectors. (f) PVK(PCBM) based MSM structure photodetectors.

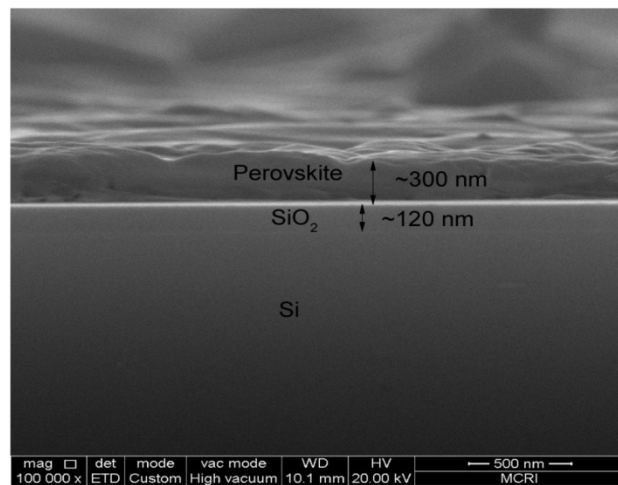


Figure S7. Cross-section SEM image of Si (heavily doped)/ SiO_2 /perovskite MOS structure.

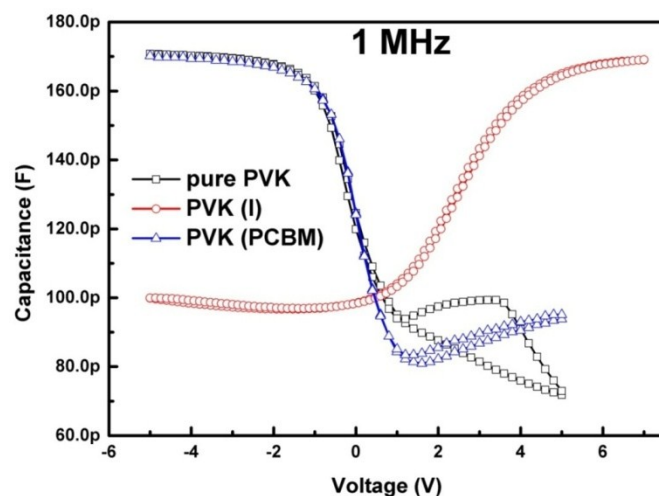


Figure S8. High frequency capacitance versus gate voltage (Al electrodes) of three kinds of perovskite based MOS capacitors.

Table S1. Table summarizing the parameters obtained from fits to the time-resolved photoluminescence data in Figure 1 using functions of the form $B1\exp(-t/\tau1) + B2\exp(-t/\tau2)$. χ^2 represents the reduced chi-squared value, the closer this value is to 1, the more accurate the fit.

Perovskite	Temperature (K)	B1	$\tau1$ (ns)	B2	$\tau2$ (ns)	χ^2
Pure PVK	300	558.139	9.5659	2093.061	66.8681	1.095
	77	0.2632	7.94	1.1820	37.82	1.125
PVK (I)	300	16.480	0.3855	2162.319	8.5740	1.616
	77	0.1903	7.27	1.3515	35.93	1.004
PVK (PCBM)	300	810.303	8.5299	1937.089	49.2816	1.069
	77	0.3379	19.48	0.7284	56.14	1.085

Table S2. The mobilities of perovskites with different measurement methods under different conditions in previously other's reports.

Sample configuration	Method	Conditions	Mobility (cm ² /Vs)	Ref.
PCBM-doped MAPbI ₃	Hall Effect	300 K	35.5	¹
undoped-MAPbI ₃			16.9	
MAPbI ₃ (TiO ₂ or Al ₂ O ₃)	TRMC	300 K, 23 GHz	67.5 ± 7.5	²
MAPbI ₃ (TiO ₂ or Al ₂ O ₃)	THz	300 K	16.25 ± 8.75	³
	TRMC	300 K, 8.45 GHz	2 ± 1	
	TA	300 K	25	
MAPbI _{3-x} Cl _x	THz	300 K, 10 THz	~27 ± 3	⁴
		77 K, 10 THz	~150 ± 17	
MAPbI ₃	TRMC	300 K, 12 GHz	6.2 ± 0.7	⁵
		165 K, 12 GHz	16.0 ± 1.7	
MAPbI _{3-x} Cl _x	FET	300 K	μ_e : 1.0 ± 0.1, μ_h : 1.3 ± 0.1	⁶
MAPbI ₃	FET	78 K	7.2×10 ⁻² , 2.1×10 ⁻²	⁷
MAPbBr ₃	Hall Effect	300 K	60	⁸
MAPbI ₃	TPC	300 K	1.9×10 ⁻³	⁹
MAPbI ₃ /PCBM			2.4×10 ⁻³	
MAPbI ₃ single crystal	SCLC	300 K	μ_h : 164 ± 25	¹⁰
	TOF		μ_e : 24.0 ± 6.8	
MAPbI ₃ single crystal	TOF	300 K	115	¹¹
	Hall Effect		40 ± 20	
	SCLC		2.5 ± 0.3	
MAPbI _{3-x} Cl _x	TRPL	300 K	μ_e : 1.6 ± 0.6, μ_h : 2.1 ± 0.8	¹²
MAPbI ₃			μ_e : 0.7 ± 0.4, μ_h : 0.4 ± 0.3	
MAPbI ₃	TA	300 K	μ_e : 1.38, μ_h : 0.85	¹³
MAPbI ₃	FET	300 K	μ_e : 0.5 ± 0.2	¹⁴
		100 K	μ_e : 5 ± 1	

Table S3. Table summarizing the parameters obtained from fits to the rise and fall time of the MOS structure photodetectors and the MSM structure photodetectors in Figure 2 using the exponential decay equation.

Perovskite	Structure	Rise time (ms)		Fall time (ms)	
		τ_{r1}	τ_{r2}	τ_{f1}	τ_{f2}
Pure PVK	MOS	1.82±0.02	8.02±0.02	2.49±0.01	6.09±0.01
	MSM	1.19±0.01	2.52±0.01	1.43±0.01	3.41±0.01
PVK (I)	MOS	4.29±0.03	13.51±0.03	6.88±0.02	15.26±0.02
	MSM	1.67±0.02	11.33±0.02	1.01±0.02	2.68±0.02
PVK (PCBM)	MOS	0.72±0.02	1.59±0.02	1.28±0.02	2.23±0.02
	MSM	0.56±0.03	1.77±0.03	0.96±0.03	1.95±0.03

REFERENCE

1. H. Jiang, G. Jiang, W. Xing, W. Xiong, X. Zhang, B. Wang, H. Zhang and Y. Zheng, *ACS Appl. Mater. Interfaces*, 2018, **10**, 29954-29964.
2. H. Oga, A. Saeki, Y. Ogomi, S. Hayase and S. Seki, *J. Am. Chem. Soc.*, 2014, **136**, 13818-13825.
3. C. S. Poncea, Jr., T. J. Savenije, M. Abdellah, K. Zheng, A. Yartsev, T. Pascher, T. Harlang, P. Chabera, T. Pullerits, A. Stepanov, J. P. Wolf and V. Sundstrom, *J. Am. Chem. Soc.*, 2014, **136**, 5189-5192.
4. M. Karakus, S. A. Jensen, F. D'Angelo, D. Turchinovich, M. Bonn and E. Canovas, *J. Phys. Chem. Lett.*, 2015, **6**, 4991-4996.
5. T. J. Savenije, C. S. Poncea, Jr., L. Kunneman, M. Abdellah, K. Zheng, Y. Tian, Q. Zhu, S. E. Canton, I. G. Scheblykin, T. Pullerits, A. Yartsev and V. Sundstrom, *J. Phys. Chem. Lett.*, 2014, **5**, 2189-2194.
6. Y. Mei, C. Zhang, Z. V. Vardeny and O. D. Jurchescu, *MRS Commun.*, 2015, **5**, 297-301.
7. X. Y. Chin, D. Cortecchia, J. Yin, A. Bruno and C. Soci, *Nat. Commun.*, 2015, **6**, 7383.
8. M. I. Saidaminov, V. Adinolfi, R. Comin, A. L. Abdelhady, W. Peng, I. Dursun, M. Yuan, S. Hoogland, E. H. Sargent and O. M. Bakr, *Nat. Commun.*, 2015, **6**, 8724.
9. Y. Shao, Z. Xiao, C. Bi, Y. Yuan and J. Huang, *Nat. Commun.*, 2014, **5**, 5784.
10. Q. Dong, Y. Fang, Y. Shao, P. Mulligan, J. Qiu, L. Cao and J. Huang, *Science*, 2015, **347**, 967-970.
11. D. Shi, V. Adinolfi, R. Comin, M. Yuan, E. Alarousu, A. Buin, Y. Chen, S. Hoogland, A. Rothenberger, K. Katsiev, Y. Losovskyj, X. Zhang, P. A. Dowben, O. F. Mohammed, E. H. Sargent and O. M. Bakr, *Science*, 2015, **347**, 519-522.
12. S. D. Stranks, G. E. Eperon, G. Grancini, C. Menelaou, M. J. Alcocer, T. Leijtens, L. M. Herz, A. Petrozza and H. J. Snaith, *Science*, 2013, **342**, 341-344.
13. G. Xing, N. Mathews, S. Sun, S. S. Lim, Y. M. Lam, M. Gratzel, S. Mhaisalkar and T. C. Sum, *Science*, 2013, **342**, 344-347.
14. B. Y. Satyaprasad P. Senanayak, Tudor H. Thomas, Nadja Giesbrecht, Wenchao Huang, Eliot Gann, Bhaskaran Nair, Karl Goedel, Suchi Guha, Xavier Moya, Christopher R. McNeill, Pablo Docampo, Aditya Sadhanala, Richard H. Friend, Henning Sirringhaus, *Sci. Adv.*, 2017, **3**, e1601935.